Fresenius J Anal Chem (1996) 354:823–828

AWARDED POSTER

D. Wienke · W. van den Broek · W. Melssen
L. Buydens · R. Feldhoff · T. Huth-Fehre · T. Kantimm
F. Winter · K. Cammann

Near-infrared imaging spectroscopy (NIRIS) and image rank analysis for remote identification of plastics in mixed waste

Received: 29 June 1995 / Accepted: 22 September 1995

Abstract An infrared camera with focal plane InSb array detector has been applied to the characterization of macroscopic samples of household waste over distances up to two meters. Per waste sample (singelized), a sequence of images was taken at six optical wavelength ranges in the near infrared region (1100 nm – 2500 nm). The obtained three-dimensional data stack served as individual fingerprint per sample. An abstract factor rotation of this stack of six images into a spectroscopical meaningful intermediate six-element vector by Multivariate Image Rank Analysis (MIRA) finally provided a decision limit for the discrimination of plastics and nonplastics. A correct classification of better than 80% has been reached. The experimental NIRIS set-up has been automated so far to allow an on-line identification of a real world waste sample within a few seconds.

Introduction

Near-and Mid-Infrared Imaging Spectroscopy (NIRIS, MIRIS) are young and upcoming analytical techniques. They form alternatives to Raman imaging spectroscopy. Future expected specific advantages of NIRIS (resp. MIRIS) are high speed and high sensitivity. A few years ago, Robert et al. [1], McClure [2, 3] and Geladi et al. [4] started to use NIRIS for qualitative and quantitative image analysis of distinct organic and inorganic materials. They mainly used the optical near infrared short-wave region below 1700 nm. Mainly slow-scan videcon type cameras were available. Recently semiconductor materials (InGaAs, InSb, HgCdTe) became available from military infrared imaging technology for civil research as focal plane array cameras containing rectangular arrangements of many thousands of miniaturised infrared sensitive detector elements. Distinct grades of these advanced detector materials not only cover the entire optical NIR wavelength range (800–2500 nm), but also parts of the mid-infrared wavelength range. Additionally, these materials offer the new possibility for rapid acquisition of at least fifty infrared images per second. In this way, these infrared cameras became attractive for real-time observations of chemical reactions and processes. Recently, Lewis, Levin and Treado [5, 6, 7] reported first results with their InSb focal plane diode array for spectroscopic NIR- and MIR-microscopy. Lodder [8] reported a comparison of an InSb array versus a PtSi CCD array camera for medical NIR imaging. Marcott and Reeder [9] proposed the use of NIRIS in a process-analytical industrial environment.

A macroscopic application with a similar InSb camera type has been reported by us [10, 11, 12, 13] for rapid presorting of household waste over a measuring distance of up to two meters. InSb is optically sensitive between 1.1 µm and 5.5 µm which provides for simultaneous NIRIS and MIRIS experiments. Chemometrical methods were used by the present authors to select the optimal subset of wavelengths and to decompose and to analyse the images. The aim of this work is to identify plastics in the waste stream by using the InSb focal plane array as remote material sensitive image sensor. The enormous camera speed and the possibility to extract spectroscopic fingerprints of single samples and to get simultaneously local image information of shape and size of a sample are obvious advantages compared to a classical NIR (resp. MIR) spectrometer. After the first feasibility studies [11, 12], the present work continues with a more quantitative evaluation of the developed macroscopic set-up. Two additional wavelength regions were added to the image stack to improve the spectroscopic discrimination between plastics and non-plastics. The entire set-up has been automated now by triggering the used filter wheel and by real-time acquisition and on-line processing of the image sequence per sample. A recently developed method MIRA (Multi-

D. Wienke (✉) · W. van den Broek · W. Melssen · L. Buydens
Catholic University of Nijmegen,
Laboratory of Analytical Chemistry, Toernooiveld 1,
NL-6525 ED Nijmegen, The Netherlands

R. Feldhoff · T. Huth-Fehre · T. Kantimm · F. Winter
K. Cammann
Institute for Chemical and Biochemical Sensors Research
(ICB Münster), Mendel-Strasse 7, D-47075 Münster, Germany

variate Image Rank Analysis) [12] was implemented among other classifiers for on-line identification of a macroscopic sample. An increased collection of 51 real-world waste samples (plastics and non-plastics) of different grades, size, color, thicknesses and surface quality were quantitatively analysed.

Theory

A final netto (near)-infrared image, **I** (dimension $n \times m$), of a chemical sample forms a data matrix of intensity values, measured simultaneously at $n \times m$ pixels (representing the photonic current per detector element of the focal plane array). **I** is obtained by correcting the socalled primary brutto image, $\mathbf{I}^{reference\,+\,sample}$ with an empty reference image of the neutral background, $\mathbf{I}^{reference}$ and a so-called dark current level image of the focal plane array detector itself, $\mathbf{I}^{dark}$, according to

$$\mathbf{I} = 1 - (\mathbf{I}^{reference\,+\,sample} - \mathbf{I}^{dark}) \,/\, (\mathbf{I}^{reference} - \mathbf{I}^{dark}) \qquad (1)$$

Similar to spectroscopic absorbance (resp. reflectance) measurements, Eq. (1) corrects for the detector off-set and for the spectral characteristics of the focal plane array, for inhomogeneous background, for an inhomogeneous illumination spectrum of the used illumination source as well as for the absorbance spectrum of the camera optics.

The resulting netto image, **I**, then shows the sample within the image by significantly higher values then zero. The surrounding background pixels have intensity values close to zero (Fig. 1).

If an optical dispersive element (prism, interference filters, grid, acousto-optical tunable filter (AOTF)) is placed in front of the focal plane array detector, several netto images, $\mathbf{I}_l$, at different wavelengths $l = 1 \ldots p$ can be taken from the same object. According to the absorbance (resp. reflectance) characteristics of the sample material at this particular wavelength, the image intensities will vary from image to image following the sample spectrum at each local sample position (Fig. 1). Thus, if one measures per sample an image at p distinct wavelengths, one obtains a so called three-dimensional stack of p images (Fig. 1). A capitalised, underlined bold letter $\underline{\mathbf{X}}$ (dimension $n \times m \times p$) is used for such a three-dimensional data array. Two directions of this data stack origin from image geometry $n \times m$ and the third direction from the p distinct wavelengths. One way, to get information about the searched type of same material is a decomposition of this image stack by Multivariate Image Rank Analysis (MIRA). MIRA is a modified singular value decomposition algorithm. It makes use of the pre-processing step in Eq. (1) assuming that most variation in the image stack is caused by the sample pixels. Background pixels are expected to scatter around zero values. Other sources of variation such as noise, distinct types of shadow and spikes from dead pixels of the focal plane array should exhibit a significant lower level of variation. Under these experimental assumptions, MIRA will provide not only an abstract singular value decomposition, but also a certain factorial rotation of the three-dimensional image stack towards a spectroscopically interpretable solution. The dominating rank-1 component will always carry the information about the sample material. The remaining rank components will contain information about shadow, noise, background variation and other minor image effects.

The MIRA algorithm works as follows:

1. unfold $\underline{\mathbf{X}}$ into matrix $\mathbf{Z}$ of p columns and $n \times m$ rows
2. perform a singular value decomposition of the squared matrix $(\mathbf{Z}^T\mathbf{Z})$ providing three abstract matrices $\mathbf{U}$ = eigenvectors $(\mathbf{Z}^T\mathbf{Z})^T(\mathbf{Z}^T\mathbf{Z})$, matrix $\mathbf{E}$ = eigenvectors $(\mathbf{Z}^T\mathbf{Z})(\mathbf{Z}^T\mathbf{Z})^T$ and λ = diagonal matrix of singular values
3. select the rank-1 component vector $\mathbf{u}_1$ from $\mathbf{U}$ (resp. $\mathbf{e}_1$ from $\mathbf{E}$, because they are identical). Its elements will show a normalised mini-spectrum of the sample
4. calculate from $\mathbf{u}_1$ (resp. $\mathbf{e}_1$) the decision criterion

$$B^{sample} = \left(\sum_{k=1}^{p/2} \mathbf{u}^2_{k,\,peaks} \Big/ \sum_{k=1}^{p/2} \mathbf{u}^2_{k,\,valleys} \right) \qquad (2)$$

which provides the multivariate ratio of high absorption peaks to low absorption peaks. To get correct results for MIRA, in total p wavelengths have to be selected at $p/2$ positions with strong absorption peaks and at $p/2$ wavelengths corresponding to low absorption 'valleys'.

The value for B will represent spectra with high peaks in the near-infrared range (for example for plastics) significantly larger than one. For spectra with 'flat' absorbance profiles in the NIR, B will be close to one or significantly smaller than one (for example for non-plastics such as glass or metal). In this way, the former original 3-dimensional data array, $\underline{\mathbf{X}}$, from the camera measurement of one waste sample is compressed to a single number B as a scalar decision limit for future control of an automated waste sorter.

Experimental set-up

The central part forms an InSb focal plane diode array camera IRC-64 (Cincinatti Electronics Inc., Ohio, USA). It has been mounted at an optical bench on the laboratory wall and equipped with a triggered filter wheel. A high-speed 16-bits digital interface S16D (EDT Inc., Oregon, USA) allows real-time data acquisition of 52 images/s by a SUN Spare 10 (Unix workstation). The real-time measurement is done under the large KHOROS imaging software package (University of New Mexico, Albuquerque, USA). Communication software between the S16D card and KHOROS and the electronic installation has been realised by Starling Consultancy (Hengelo, The Netherlands). Complete infrared movies can be measured by the IRC-64 and then presented by KHOROS by real-time visualisation of the movie out of the workstation's RAM. IRC-64 images can be saved to disk in several formats by KHOROS. In this way the images can be read into other imaging software, such as MATLAB, and into self-developed programmes under the Unix operating system. For the present NIRIS experiments, the filter wheel has been equipped with six NIR interference filters (Spectrogon (Sweden), Fairlight (UK)) with the following wavelength ranges: narrow band pass filter 1 (1600 ± 110 nm), narrow band pass filter 2 (1700 ± 90 nm), broad band filter 3 (1700–2150 nm), broad band filter 4 (2115–2550 nm), narrow band pass filter 5 (1562 ± 32 nm), narrow band pass filter 6 (2200...2300 nm). Further equipment such as a pin-hole set up,

mirrors and (N)IR-illumination sources were mounted. The pixel-wise recalibration of the camera is done by a so-called uniformity module using a cool and a hot emission source. A sanded aluminium plate served as homogeneous background and to get the required reference images per wavelength region. Further details about the entire experimental set-up were given, for example, in [11, 12].

Software and computations

Images of the sample were recorded by the KHOROS software on-line from the camera. The MIRA algorithm as described in the theoretical part, has been completely developed and implemented in MATLAB. MIRA has been also implemented and tested in C language for the hardware set-up in one-line mode. This allows to use MIRA outside KHOROS by direct access in real-time and in on-line mode to the IRC-64 camera to run the complete pre-sorter set up automatically.

Materials and methods

The sample collection covered 51 macroscopic samples containing 23 plastics (5 × polyethylene (PE), 6 × polypropylene (PP), 5 × polyethyleneterephthalate (PET), 4 × polystyrene, 3 × polyvinylchloride (PVC)) and 28 non-plastics (2 × cotton (TEX), 4 × glass (GLS), 6 × metal (MET), 7 × (PAPER), 5 × (WOOD), 4 × ceramics (CER)). Samples vary in size (between 1–5 cm), shape (circular, rectangular, irregular, etc.), color (transparent, white, yellow, dark blue, etc.), thickness (thin sheets, thick bulks, hollow bodys, etc), and surface quality (rough, coated, printed, reflecting, flat, structured, etc). A sequence of $p = 6$ NIR-images (size $n = 64$, $m = 64$ pixels) was recorded from each sample. Additionally, a dark current image of the focal plane array detector and six reference images were taken for correction of each sample image according to Eq. (1). Each three-dimensional image stack $\mathbf{X}$ of size 64 × 64 × 6 pixels, belonging to one sample, has been unfolded to the corresponding matrix $\mathbf{Z}_{4096,6}$. From its corresponding 6 × 6 matrix $\mathbf{Z}^T\mathbf{Z}$, the MIRA algorithm provided the B-value as basis for a decison for the correct type of material of the considered sample. The total observed computation time (including pre-processing of the 13 images and MIRA) concerned only a few milliseconds per waste sample.

Typical near-infrared images of a plastic sample (polystyrene) and a piece of non-plastic (metal lead) are presented in Fig. 1. The piece of plastic has a hole at its lower left side and a sticker of paper at its upper right side. The images were taken with a InSb focal plane diode array camera and the experimental set-up described in the experimental section. Lead shows no difference in absorption for the two chosen NIR wavelength regions. In contrast to that, the piece of polystyrene shows strong differences in absorption corresponding to its NIR spectrum.

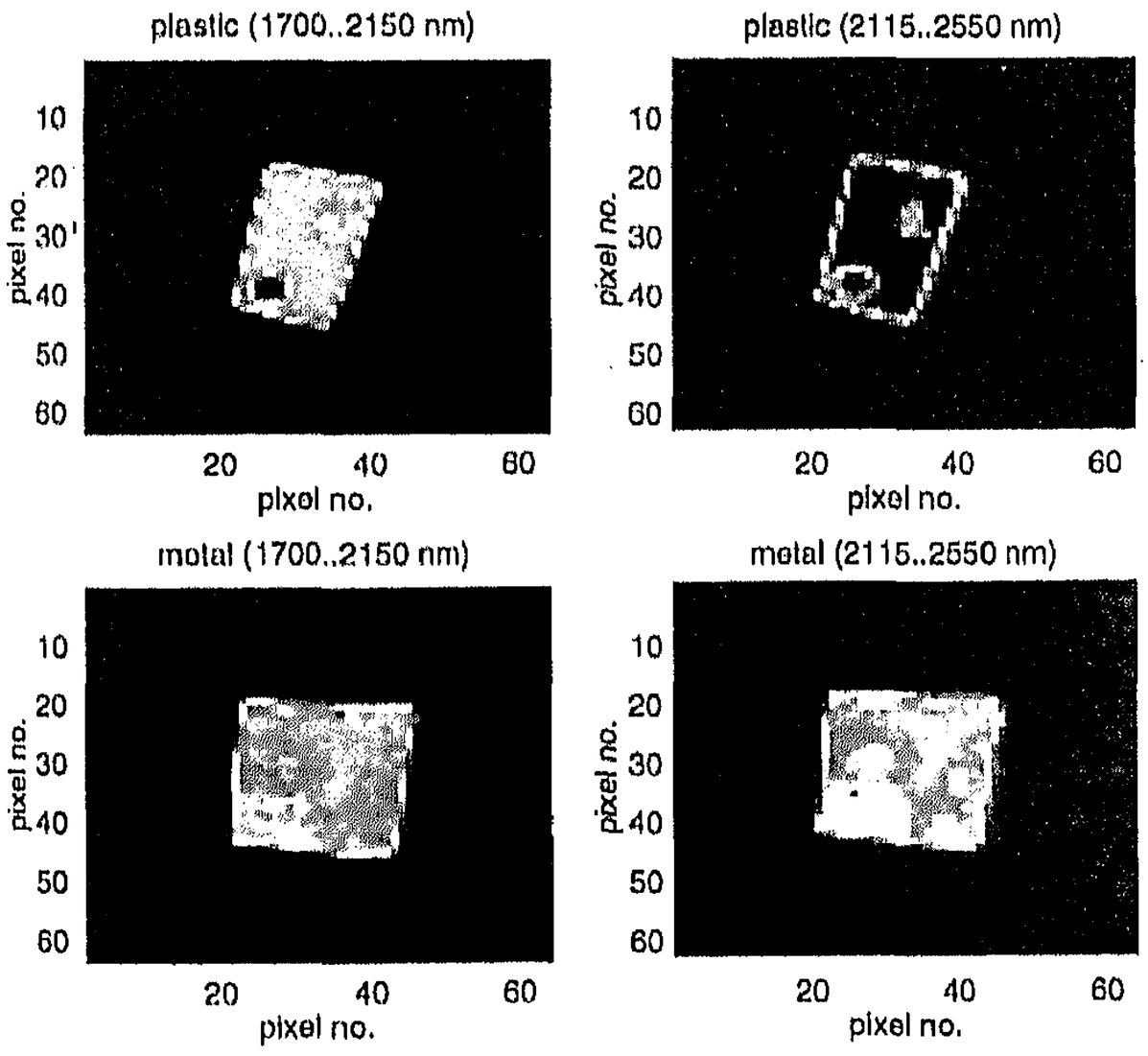

Fig. 1 Typical near-infrared images of a plastic sample (polystyrene, *both upper images)* and a piece of non-plastic (metal lead, both lower images)

Results and discussion

Pattern recognition results by MIRA

The individual sets of singular values for each of the by MIRA analysed 51 image stacks are clearly dominated by the significant size of the first singular value (Table 1). If the first singular value obtained (λ_1) is significantly larger than the remaining singular values, it can be expected that the corresponding eigenvector $\mathbf{u}_1$ will match the correct spectral pattern of the sample material. This is an indication, that in all cases the main variation in the image is caused by one dominating rank-1 component. Homogeneous illumination and background-to-zero correction according to Eq. (1) ensured that the rank-1 component in all image stacks became identical with the sample signal itself as main source for data variation. Together with the significant size of the first singular value, the profile $\mathbf{u}_1$ of the corresponding first singular vector can be considered. $\mathbf{u}_1$ should look like a normalised NIR mini-spectrum of the sample (Fig. 2).

If both conditions (dominant first singular value, correct rotated $\mathbf{u}_1$-profile) are fulfilled, the B-value can be calculated (Fig. 3). The larger B, the more characteristic and the less 'flat' the normalised mini-spectrum $\mathbf{u}_1$ is. The B-values for all 23 plastics (Fig. 3a) and for all 28 non-plastic samples (Fig. 3b) show a significant difference. Most of the plastic's B-values are larger than the total median (MT = 1.59) of both material groups. In contrast to that, the majority of non-plastic's B-values are below MT. The medians of plastics (MP = 2.26) and of non-plastics (MN = 1.28) differ significantly. However, there are eight exceptions. The non-plastic samples (PAPER (2–4, 7) show larger B-values than MT. The three plastic samples PE(2), PET(%) and PP(5) have B-values below MT. From the point of view of recycling technology, the latter problem is much less critical than the first one. If the total median of B-values MT would be used as a decision border, whether a sample at the conveyor belt is made from plastic or not, a classification error of 5/28 false positive answers would have been given. This would mean a purity of the presorted plastic waste of 82.1%. This purity level – although still low – is already interesting for further recycling applications and it is highly comparable with the sorting quality reached by hand-picking driven waste sortation plants. Looking more in detail to the wrong classified eight non-plastic samples it is to see that these are only 'natural' polymers such as paper and wood. Glass, metal,

Table 1 23 plastic and 28 non-plastic samples, their characteristics and corresponding six singular values, extracted by MIRA from the NIR image stack per sample

Sample no.	Sample identifier	Main features color	Corresponding eigenvalue					
			λ_1	λ_2	λ_3	λ_4	λ_5	λ_6
1	PE1	white, thick	975.9	16.24	13.24	7.3	5.4	2.0
2	PE2	white, thick	1469.2	13.7	10.8	6.1	4.2	2.0
3	PE3	transparent, thin	1419.1	109.8	8.4	4.0	1.6	1.1
4	PE4	yellow, thick	1000.9	180.2	10.7	4.2	1.3	0.8
5	PE5	blue, thin	40.51	13.9	5.59	2.51	1.29	0.54
6	PET1	transparent, thin	203.5	11.8	6.7	2.7	2.1	1.5
7	PET2	white-thin	199.9	26.0	13.6	8.2	5.6	1.4
8	PET3	beige, thin	340.1	8.6	6.6	4.3	2.5	0.8
9	PET4	transparent, thin	153.8	29.7	7.8	3.9	0.9	0.3
10	PET5	transparent, thin	178.0	37.5	22.0	13.1	7.1	5.8
11	PP1	white, thin	355.7	18.1	7.13	5.5	3.7	1.6
12	PP2	yellow, thin	473.7	19.7	7.8	4.8	3.3	0.6
13	PP3	white, thick	1150.1	10.9	10.1	0.0	0.0	0.0
14	PP4	yellow, thin	654.2	23.18	12.0	6.5	1.8	1.2
15	PP5	white, thick	502.0	20.0	13.6	6.3	3.0	0.5
16	PP6	transparent, thin	168.2	21.6	7.5	3.8	2.8	0.6
17	PS1	white, thin	478.1	13.8	7.1	6.2	1.4	0.7
18	PS2	transparent, thick	338.0	16.2	9.5	3.9	1.8	1.1
19	PS3	blue, thin	288.2	7.4	6.0	2.8	2.3	0.9
20	PS4	white, thin	532.2	16.4	9.9	5.7	4.4	0.6
21	PVC1	beige, thick	120.6	12.6	4.8	2.6	1.0	0.5
22	PVC2	white, thick	261.9	42.0	7.1	3.7	1.7	0.5
23	PVC3	yellow, thick	192.7	22.0	7.1	3.8	1.6	0.7
24	PAPER1	brown, thin	986.4	13.7	9.7	7.2	1.2	0.9
25	PAPER2	black, thin	831.1	11.8	8.2	6.0	1.6	0.8
26	PAPER3	white, thin	466.5	14.3	4.8	3.0	2.0	1.0
27	PAPER4	colored, smooth	798.4	28.0	10.7	3.7	1.3	0.7
28	PAPER5	colored, thin	497.4	15.5	9.2	3.8	1.6	0.6
29	PAPER6	grey, smooth	926.8	31.7	21.4	8.1	6.4	3.2
30	PAPER7	colored, smooth	137.7	13.6	8.9	6.0	2.5	0.5
31	WOOD1	thick	1004.2	11.6	10.0	5.6	1.0	0.7
32	WOOD2	thick	246.0	8.2	5.5	3.7	2.8	0.8
33	WOOD3	cork, thick	511.7	11.3	7.5	4.8	3.3	1.5
34	WOOD4	thick	483.4	14.3	5.8	3.8	2.1	1.0
35	WOOD5	thin, black ink	483.4	14.3	5.8	3.8	2.1	1.0
36	TEX1	black, cotton + nylon	1869	16.8	8.9	4.6	1.6	0.8
37	TEX2	beige cotton	341.6	6.6	5.3	3.8	2.2	0.7
38	GLS1	transparent, thick	118.9	14.4	4.3	2.8	1.4	0.6
39	GLS2	transparent, thin	137.5	18.5	13.4	8.7	6.5	2.1
40	GLS3	green,thick	438.4	16.2	7.6	6.6	4.8	1.8
41	GLS4	brown, thick	928.0	13.0	10.7	5.9	5.5	1.7
42	CER1	thick, white, ink	277.2	41.1	29.4	15.4	10.0	2.6
43	CER2	thick, white	1347.1	149.7	9.2	4.9	1.7	0.08
44	CER3	thick, white + blue	1717.1	29.2	17.6	8.5	2.1	0.8
45	CER4	china porcelain	350.2	19.3	8.6	4.0	2.4	1.0
46	MET1	stainless steel, thin	1364.2	372.1	331.3	195.7	151.2	60.5
47	MET2	thick aluminium	1395.2	18.7	10.1	8.1	1.6	0.0
48	MET3	tin, thick	287.9	16.3	8.5	5.0	1.5	0.8
49	MET4	lead, thick	528.1	41.6	7.3	4.7	1.8	0.5
50	MET5	aluminium can, colored	2010.1	158.2	53.9	40.4	13.2	8.1
51	MET6	copper, thick	1838.5	742.7	314.6	186.4	38.5	5.8

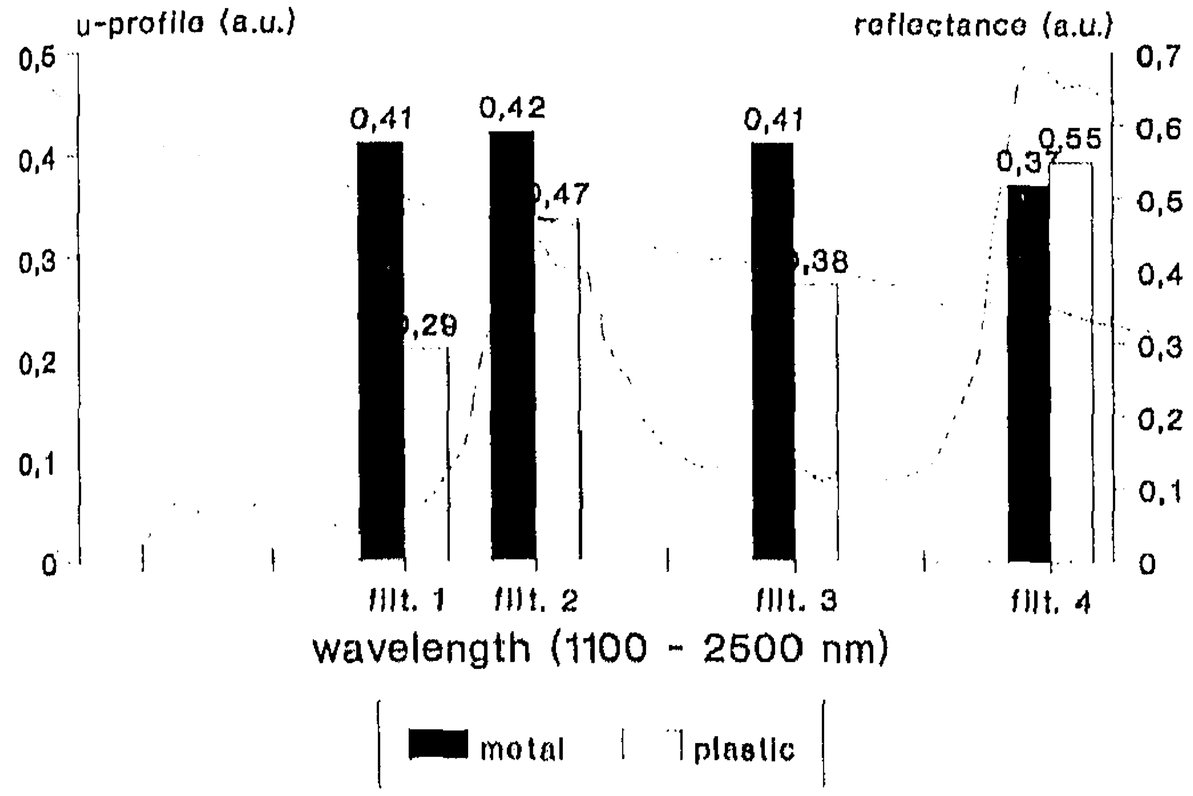

Fig. 2 Graphical comparison of the NIR spectra of the metal sample MET4 *(solid line)* and of the plastic sample PS1 *(dotted line)* (for their NIR images see Fig. 1) with the profile of the $\mathbf{u}_1$-vector. $\mathbf{u}_1$ has been extracted by MIRA from the $64 \times 64 \times 6$ three-dimensional image stack of each sample

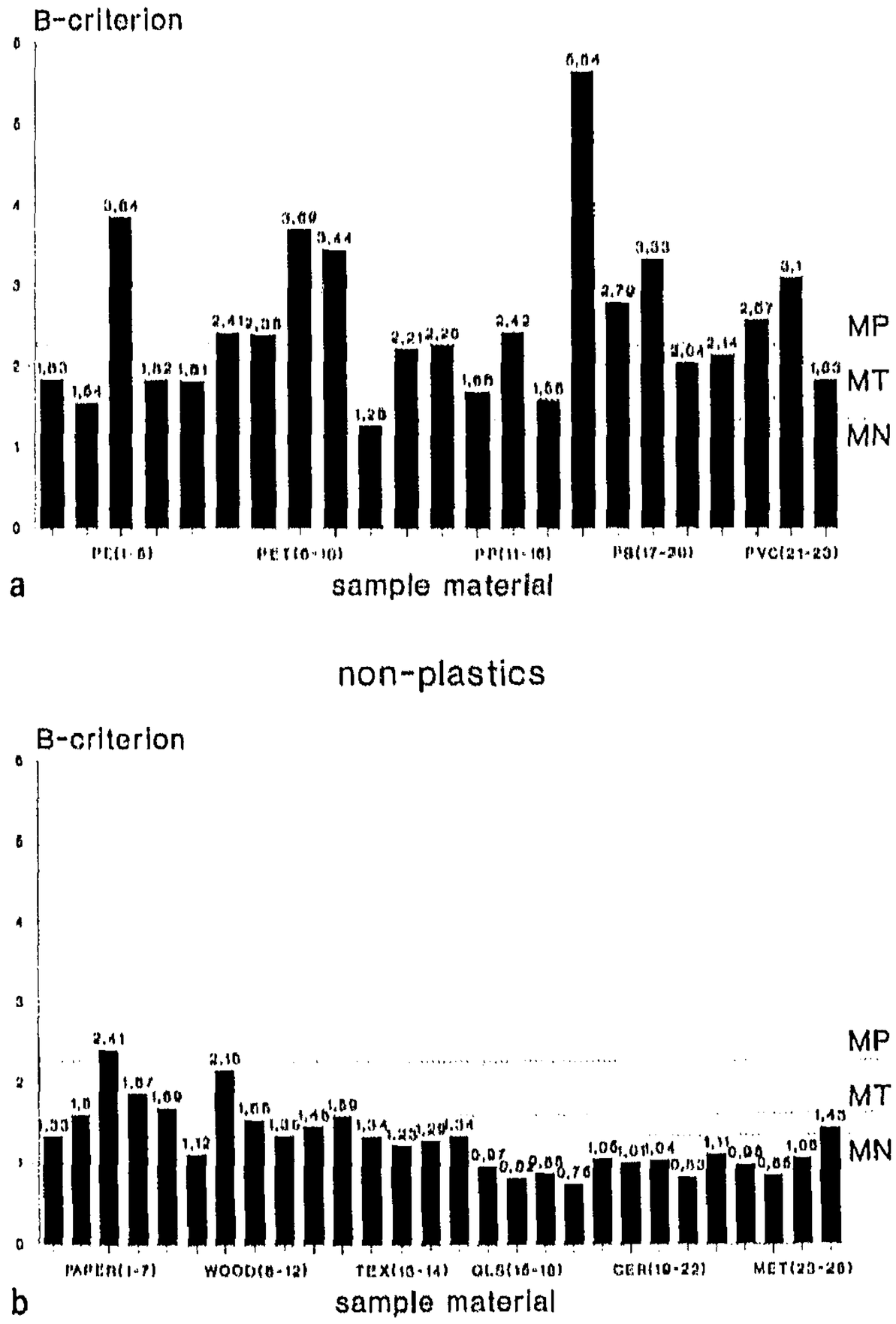

Fig. 3a, b Bar chart presentation of the size of experimental B-criteria, obtained by a multivariate image rank analysis (MIRA) for each individual sample of 23 plastics and 28 nonplastics

ceramics and non-plastic textiles were always correctly identified. More specific, the wrongly classified samples PAPER (3) and PAPER(7) have a smooth plastified surface (mostly PE or PP) what explains their significant high B-values of 2.41 and 2.16. In fact, these samples represent a multilayer-system of paper and plastic. Recently it was shown [14, 15], that these combination materials can easily be separated from plastics in a subsequent fine-sorting step by using full size NIR spectra. Obviously the limited number of six filters in front of the focal plane array camera does not provide enough spectroscopical information for a safe separation of plastified materials from pure plastics. The other three misclassified samples PAPER (2,4,5) were coated with black and colored ink what partly explains their high spectral responses. Such inks often contain organic polymer components. However, the overall result shows that the total median MT of B-values, for example, could be a suitable decision border whether a waste sample belongs to the group of plastics or to the group of non-plastics.

Factorial image decomposition by MIRA

An example for factorial image decomposition is given in Fig. 4. After a MIRA decomposition of the $p = 6$ images of a piece of polystyrene (PS1) (partly shown in Fig. 1, upper two original images), a set of new 'singular' images was obtained. Before discussing these six new images more in detail, the mathematical way of reconstruction will be shortly illustrated. Similar to related studies, carried out by Geladi and others [16, 17, 18, 19] it can be shown, that

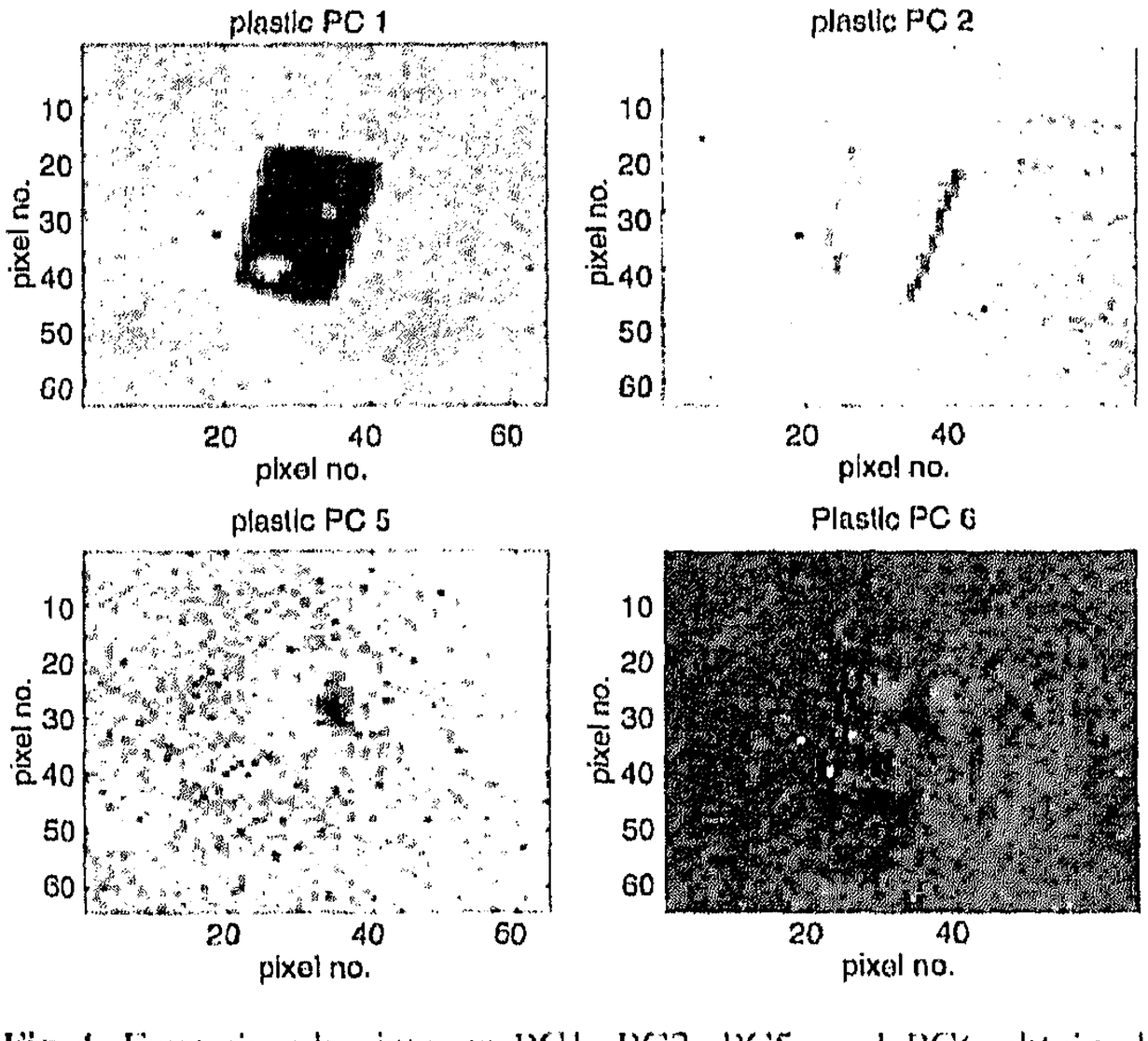

Fig. 4 Four singular images PC1, PC2, PC5, and PC6 obtained from multivariate image rank analysis of a three-dimensional array of $p = 6$ images of a sample of polystyrene (PS1, selected original NIR images of this sample given in Fig. 1, *top*)

the orthonormal matrix of singular vectors **E**, obtained from the singular value decomposition of a matrix $\mathbf{Z} = \mathbf{X}^T\mathbf{X}$, into

$$\mathbf{Z} = \mathbf{UVE}^T \tag{3}$$

is identical to the matrix **E**, obtained from a direct singular decomposition of the matrix **X** according to

$$\mathbf{X} = \mathbf{SVE}^T \tag{4}$$

Further, both decompositions agree in their p × p dimensional diagonal matrix **V** of singular values. In the upper case (Eq.3), additionally both matrices **U** and **E** are identical. Using this knowledge, the product matrix $\mathbf{S} \times \mathbf{V}$ of normalised scores of individual image pixels can be estimated by a multiple linear regression step

$$\mathbf{S} \times \mathbf{V} = ((\mathbf{U}^T\mathbf{U})^{-1}\mathbf{U}^T\mathbf{X}^T)^T \tag{5}$$

which can be simplified, based on the orthonormal properties of **U**, into

$$\mathbf{S} \times \mathbf{V} = (\mathbf{U}^T\mathbf{X}^T)^T \tag{6}$$

Each of the p columns of the normalised scores matrix $\mathbf{S} \times \mathbf{V}$ contains then an unfolded 'singular image'. These p unfolded images are ranked according their decreasing variance contributions to the original images. From these p columns, the 'singular images' are obtained by folding them back to the normal n × m image size and visualising them.

Returning back to the example in Fig. 4, it can be seen that the first singular image PC1 shows the typical contours of the PS sample with its hole at its left lower corner and a sticker of paper at its upper right hand side. Paper and polystyrene seem difficult to separate with these 6 chosen filters so that they are still seen together in image PC1. This agrees with the former pattern recognition results. The singular value images PC2–PC4 show distinct types of shadows and/or image mismatches at the sample borders. These sample mismatches (1–2 pixels) origine from relative sample movements during the measurements. An interesting detail is to see in the singular value image PC5. Obviously the paper sticker provided slightly deviating spectral information which allows to separate it from the shadow and from the sample. However, its variance contribution is very small compared to the total variance distribution in sample PS1 (compare singular values in Table 1 for PS1). The remaining sixth singular image PC6 in Fig. 4 only shows the noise of the measurement (random image pattern) at a very low level. The demonstrated possibility of pixelwise image decomposition by MIRA offers, in principle, also a future classification of each pixel to a certain class (background, shadow, sample material, etc.).

Conclusions

Multivariate image rank analysis (MIRA) can serve as a factorial rotation technique for three-dimensional data stacks of experimental near-infrared images. MIRA requires no calibration step ('model free factor rotation') because it is based on the intrinsic spectral fingerprint of the analysed material. Under well defined experimental conditions, MIRA is able to provide a rapid decision about a distinct type of material (plastic, non-plastic) that was observed by remote near-infrared imaging spectroscopy (NIRIS) at a conveyor belt. Simultaneously, the shape, the size and the sample position within the image are conserved as additional descriptors for waste recycling. It has been experimentally demonstrated, that a rapid-scan focal plane diode array camera, based on an InSb semiconductor chip, in combination with MIRA can detect plastics among non-plastics in waste with better than 80% correctness within a few seconds. The speed limit, caused by a rotating circular filter wheel, can be decreased in future by a faster dispersive optical element (e.g. AOTF), which will allow future sorting decisions in significantly less response times than a second.

Acknowledgements The authors are grateful to the Commission of European Communities for financial support of the SIRIUS project under the grant no. EVWA-CT-92-0001 in the research programme ENVIRONMENT. We are grateful to H. W. Siesler and coworkers (NIR research group, University of Essen, Germany) for measuring the transmission spectra of our different camera optics. Special thanks to our undergraduate students Kees de Crom, Arjan Kraak and Diny Rovers (all Nijmegen University) for their technical assistance and their particular contributions.

References

1. Robert R, Bertrand D, Devaux MF (1991) NIR News 2(2):9–10
2. McClure WF (1991) NIR News 2(2):8
3. McClure WF (1994) Anal Chem 66(1):43A–53A
4. Geladi P, Isaksson H, Lindquist L, Wold S, Esbensen K (1989) Chemom Intell Lab Syst 5:209–220
5. Lewis EN, Levin IA (1995) Appl Spectros 49(5):673–678
6. Treado PJ, Levin IW, Levis EN (1994) Appl Spectros 48(5): 607–615
7. Lewis EN, Levin IW (1995) PITTCON'95 conference, New Orleans, March 5–10, volume of abstracts, no 47
8. Lodder R (1995) PITTCON'95 conference, New Orleans, March 5–10, volume of abstracts, no 46
9. Marcott C, Reeder RC (1995) PITTCON'95 conference, New Orleans, March 5–10, volume of abstracts, no 45
10. Wienke D, van den Broek W, Melssen W, Buydens L, Huth-Fehre T, Kantimm T, Feldhoff R, Winter F, Cammann K (1995) INCOM'95 Conference, Düsseldorf (Germany), Proceedings, p 479
11. van den Broek W, Wienke D, Crom K de, Melssen W, Buydens L (1995) Anal Chem 67:3753–3759
12. Wienke D, van den Broek W, Buydens L (1995) Anal Chem 67:3760–3766
13. van den Broek W, Wienke D, Kraak JCA, Melssen W, Buydens L (1995) Submitted
14. Huth-Fehre T, Feldhoff R, Kantimm T, Quick L, Winter F, Cammann K, van den Broek W, Wienke D, Melssen W, Buydens L (1995) J Molec Struct 348:143–146
15. Wienke D, van den Broek W, Schoenmakers J-W, Buydens L, Huth-Fehre T, Feldhoff R, Kantimm T, Cammann C (1995) Chemom Intell Lab Syst (submitted)
16. Geladi P, Esbensen K (1991) In: Devillers J, Karcher W (eds) SAR and environmental studies. Kluwer, Amsterdam, pp 415–445
17. Geladi P, Grahn H, Lindgren F (1991) In: Devillers J, Karcher W (eds) Applied multivariate analysis in SAR and environmental studies. Kluwer, Amsterdam, pp 447–478
18. Esbensen K, Geladi P (1989) Chemom Intell Lab Syst 7:67–86
19. Grahn H, Szevenyi NM, Roggenbuck MW (1989) Chemom Intell Lab Syst 7:87–93